

Analytical Formula of Positive Position Solution of 2PPa-PSS 3-Translational Parallel Mechanism with Low Coupling-degree and its Numerical Application

Junjie Gong^a, Wei Wei^{a,b,c*}, Sixu Peng^a, Kechen Zhang^a

^aSchool of Mechanical Engineering, Guangxi University, Nanning 530004, China

^bSchool of Mechanical and Automotive Engineering, South China University of Technology, Guangzhou, China

^cSchool of Mechanical Engineering, Guilin University of Aerospace Technology, Guilin, China

Received January 7 2021

Accepted October 18 2021

Abstract

Most of the parallel mechanisms (PM) with low coupling degree cannot directly obtain the analytical expression of the positive position solution of the PM, which makes it difficult to carry out the follow-up research on the kinematic accuracy analysis and trajectory planning of the PM. Based on the topological structure theory, this paper analyzes the position and orientation characteristic (POC), DOF and coupling degree of 2PPa-PSS PM. Afterward, the kinematic mathematical model of 2PPa-PSS PM is established based on the order single open chain of kinematic modeling principle. The moving platform of the mechanism is set as an equilateral triangle, and the intermediate variables are solved by combining the constraints of the two chains. The positive position solution of the PM in analytical form is obtained. The correctness of the kinematic model of the mechanism is verified by numerical calculation. Then, according to the positive position solution analytical expression, we can work out the complete workspace of the PM, and the significant influence of the driving increment on the attitude change of the moving platform is analyzed by using the analysis method based on the orthogonal test. According to the results of orthogonal experiment, the best driving range of the mechanism is obtained.

© 2021 Jordan Journal of Mechanical and Industrial Engineering. All rights reserved

Keywords: Positive position solution; Parallel mechanism; Coupling degree; Workspace; Orthogonal test;

1. Introduction

Motion analysis is the basic task of parallel mechanism, and position analysis is the basis of velocity analysis, acceleration analysis and other follow-up research [1]. Due to the mutual constraints between the branches and chains, the structure of the low-degree-of-freedom parallel mechanism is complex, and the positive position solution of the parallel mechanism in analytical form is difficult to be obtained. The application research of parallel mechanism [2-3] is limited to the analytical expression of inverse position solution, and it is difficult to carry out the follow-up research on the influence of its complete workspace, drive on the attitude change of moving platform and dynamic forward solution.

At present, for parallel mechanisms with non-zero coupling degree, there is not generally positive position solution analytical form. Only with special topological structure can we obtain the analytic expression of positive position solution. This kind of mechanism can be applied to space precise positioning [4-6] or attitude adjustment equipment [7-10], which has high research value [11-14]. Ma et al. [15] analyzed the kinematics and workspace of a 2-PrRS-PR(P)S parallel mechanism by using the closed-loop equation. Arian et al. [16] analyzed the kinematics

and dynamics of a three degree of freedom gantry tau robot. Cuan-Urquizo et al. [17] obtained a closed solution of the positive and inverse position solution of the 3-CUP parallel mechanism. Zeng et al. [18-19] analyzed the positive and inverse position solution, Jacobian matrix and stiffness performance of the three-translation parallel manipulator. Liu et al. [20] introduced a new 6-DOF orthogonal parallel mechanism, and its dynamic model was established to analyze the kinematic characteristics. Yan et al. [21] proposed a systematic approach for structure synthesis of parallel manipulator is based on position and orientation characteristic (POC) matrix, by which a detailed application is focused on the synthesis of 2-translation and 2-rotation parallel mechanisms. Zeng et al. [22-24] have done a lot of research on decoupling of parallel mechanism. For example, Zeng et al. [22] synthesized the rotary decoupled parallel mechanism based on the screw theory, proposed the selection principle of the input pair of the rotary driving limb, and formed the type synthesis method of the rotary decoupled parallel mechanism. Secondly, Zeng et al. [23] also proposed a decoupled 2T1R parallel mechanism, deduced the analytical solution expressions of the forward and inverse positions of the mechanism, and verified the decoupling characteristics of the mechanism; In addition, Zeng et al. [24] makes a systematic comparative analysis of 3-RPUR

* Corresponding author e-mail: 491651601@qq.com.

and 3-CPR parallel mechanisms. The results show that the coupling of parallel mechanisms has mutual effects on the workspace, dexterity, speed, payload capacity and stiffness of the mechanism.

However, there are the following problems in the study of parallel mechanism. When the coupling degree of mechanism is not zero, the positive position solution of mechanism can't be obtained directly [25]. Therefore, most of the workspace of parallel mechanism can only be solved based on the inverse position solution. However, it is difficult to obtain a complete workspace by using the analytical formula of the inverse position solution [1]. ② The input-output motion decoupling characteristics of parallel mechanism can only be qualitatively analyzed, but not quantitative analysis of the influence of each driving on the moving platform makes the motion control and trajectory planning more complex [26-27].

Based on the topological structure theory of parallel mechanism, this paper analyzes the position and orientation characteristic, DOF and coupling degree of a low coupling 2PPa-PSS 3-Translation parallel mechanism with special topological structure. The moving platform is set as an equilateral triangle, and the intermediate variables are solved by combining the constraint equations of Branch II and branch III. Based on the kinematic modeling principle of single open chain, the analytic expression positive position solution of the parallel mechanism is obtained. Based on the analytic expression of the positive position solution, the complete working space of the parallel mechanism is drawn. Afterward, the orthogonal test is designed to analyze the significant influence of the driving mechanism on the coordinate change of the moving platform, and the optimal driving range is obtained. Finally, according to the singular position of the mechanism, the index of testing the driving is obtained, which provides a reference for further optimization analysis and real-time control of the mechanism.

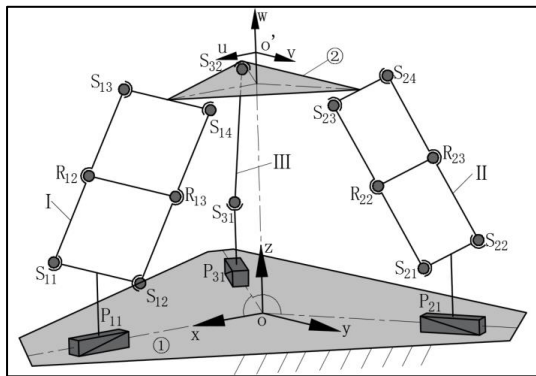


Figure 1. 2PPa-PSS Parallel Mechanism

2. Description of mechanism structure

According to the topological structure theory and design method of parallel mechanism, this paper presents a three translation parallel mechanism driven by three moving pairs, as shown in Figure 1. The whole mechanism is composed of static platform ①, moving platform ② and three branches, in which Branch I and Branch are the same hybrid single open chain (HSOC), that is, The moving pair P and the moving platform 2 are respectively connected in

the 4S parallelogram and arranged on the opposite side, which is recorded as follows $HSOC_i : P(SRS)_2 (i = I, II)$. The connection relationship of the kinematic pairs of Branch I and Branch is identical. Branch III is a single-open-chain (SOC), that is, the prismatic pair P_{31} , spherical pair S_{31} and spherical pair S_{32} are connected in series connection, they are recorded as $SOC_{III} : PSS$.

The whole mechanism is triangular and asymmetrical, which has three characteristics: simple structure, easy to manufacture and easy to assemble.

3. Analysis the topological structure of mechanism

3.1. Analysis the POC set of mechanism

The structure of hybrid single open chain I and hybrid single open chain II of the parallel mechanism is identical, and its topological structure can be expressed as:

$$C_i \{P_{i1} - \diamond(4S - 2R)\} (i = 1, 2)$$

The topological structure of single open chain III is: $C_3 \{P_{31} - S_{31} - S_{32}\}$. According to the topological structure theory and the POC equation of parallel mechanism, the POC set of mechanism is solved.

The POC equation of parallel mechanism is [25]

$$M_{bi} = \bigcup_{j=1}^k M_{sj} \tag{1}$$

$$M_{pa} = \bigcap_{i=1}^n M_{bi} \tag{2}$$

where: M_{pa} is the POC set of the mechanism moving platform; M_{bi} represent the POC set the i -th at the end of branch chain; M_{sj} denote the POC set of the j -th sub single open chain in the branch chain;

Branch I and Branch II have the same structure, and the end of them generate the POC set is identical. Owing to the motion output of parallelogram $\diamond(4S - 2R)$ is equivalent to 2T1R, according to formula (1), we can get

$$M_{bi} = \left[\begin{matrix} t^1(\|P_{i1}\|) \\ r^0 \end{matrix} \right] \cup \left[\begin{matrix} t^2 \\ r^1(\|S_{i1}S_{i2}\|) \end{matrix} \right] = \left[\begin{matrix} t^3 \\ r^1(\|S_{i1}S_{i2}\|) \end{matrix} \right] (i = 1, 2)$$

Since Branch III is an unconstrained branch, of which the end generates the POC set is

$$M_{b3} = \left[\begin{matrix} t^3 \\ r^3 \end{matrix} \right]$$

POC set of moving platform ② is

$$M_{pa} = M_{b1} \cap M_{b2} \cap M_{b3} = \left[\begin{matrix} t^3 \\ r^1(\|S_{11}S_{12}\|) \end{matrix} \right] \cap \left[\begin{matrix} t^3 \\ r^1(\|S_{21}S_{22}\|) \end{matrix} \right] \cap \left[\begin{matrix} t^3 \\ r^3 \end{matrix} \right] = \left[\begin{matrix} t^3 \\ r^0 \end{matrix} \right]$$

The result reveal that the position and orientation characteristic of any point on the moving platform ② is three translation (3TOR) which is the translation of three directions of the XYZ axis.

3.2. Calculation of degree of freedom and coupling degree of parallel mechanism

The formula of parallel mechanism is [25]

$$F = \sum_{i=1}^m f_i - \sum_{j=1}^v \xi_{Lj} \quad (3)$$

$$\xi_{Lj} = \dim. \left\{ \left(\bigcap_{i=1}^j M_{bi} \right) \cup M_{b(j+1)} \right\} \quad (4)$$

where: F is the degree of freedom of the mechanism, f_i represents the degree of freedom of the i -th kinematic pair (excluding passive degree of freedom), m denotes the number of kinematic pairs of the mechanism, n is the number of mechanism components, $v = m - n + 1$ represents the number of independent loops, ξ_{Lj} is the number of independent displacement equations of the j -th independent loop, $\bigcap_{i=1}^j M_{bi}$ denotes the *POC* set of the sub parallel mechanism composed of the first i branches, $M_{b(j+1)}$ is the set of the end components of the first $j+1$ branches.

The formula of the coupling degree κ of the mechanism is [25]

$$\begin{aligned} \kappa &= \frac{1}{2} \min. \left\{ \sum_{j=1}^v |\Delta_j| \right\} \\ &= \frac{1}{2} \min. \left\{ \sum_{j=1}^v \sum_{i=1}^{m_j} f_i - I_j - \xi_{Lj} \right\} \end{aligned} \quad (5)$$

where: $\min. \{ \}$ represents that the basic kinematic chain (BKC) is decomposed into v -th $SOC_j (\Delta_j)$, and there are many decomposition schemes, $(\sum |\Delta_j|)$ is the smallest.

The parallel mechanism can be divided into two independent circuits:

$$\begin{aligned} SOC_1 &= \{ -P_{11} \perp R_{11} \parallel \diamond (4S - 2P) \parallel R_{14} - R_{24} \parallel \diamond (4S - 2P) \\ &\parallel R_{21} \perp P_{21} - \} \\ SOC_2 &= \{ -P_{31} - S_{31} - S_{32} - \} \end{aligned}$$

According to equations (3) and (4), the number of independent displacement equations of the first independent loop is determined

$$\begin{aligned} \xi_{L1} &= \dim. \{ M_{b1} \cup M_{b2} \} \\ &= \dim. \left\{ \begin{bmatrix} t^3 \\ r^1 (\parallel R_{11}) \end{bmatrix} \cup \begin{bmatrix} t^3 \\ r^1 (\parallel R_{21}) \end{bmatrix} \right\} = 5 \end{aligned}$$

$$F_{(1-2)} = \sum_{i=1}^8 f_i - \xi_{L1} = 8 - 5 = 3$$

$$M_{pa(1-2)} = M_{b1} \cap M_{b2} = \begin{bmatrix} t^3 \\ r^0 \end{bmatrix}$$

The number of independent displacement equations of the second independent loop is

$$\xi_{L2} = \dim. \{ M_{pa(1-2)} \cup M_{b3} \} = \dim. \left\{ \begin{bmatrix} t^3 \\ r^3 \end{bmatrix} \right\} = 6$$

According to formula (3), the degree of freedom of the parallel mechanism can be obtained

$$F = \sum_{i=1}^{11} f_i - \sum_{j=1}^2 \xi_{Lj} = (8 + 6) - (5 + 6) = 3$$

The results reveal that when the three moving pairs P_{11} , P_{21} and P_{31} on the static platform ① are used as driving

pairs, the parallel mechanism can achieve 3-D translational motion output.

The constraints degrees of two single open chains are as follows

$$\Delta_1 = \sum_{i=1}^8 f_i - I_1 - \xi_{L1} = 8 - 2 - 5 = 1$$

$$\Delta_2 = \sum_{i=1}^3 f_i - I_2 - \xi_{L2} = 6 - 1 - 6 = -1$$

By substituting the results of the above two formulas into equation 5, we can get

$$\kappa = \frac{1}{2} \sum_{j=1}^2 |\Delta_j| = \frac{1}{2} (1 + |-1|) = 1$$

The results indicate that the coupling degree of the parallel mechanism is $\kappa = 1$. In most cases, it is difficult for the parallel mechanism whose coupling degree is not zero to get the analytical formula of the positive position solution of the parallel mechanism, and the parallel mechanism can get the analytical formula of the positive position solution by setting the intermediate variables.

4. Kinematic analysis of parallel mechanism

4.1. Coordinate system and parameter setting

The parallel mechanism is driven by three moving pairs P_{11} , P_{21} and P_{31} . Three driving pairs are distributed on the same platform ①, and their axis angle is 120° . According to figure 1, the kinematic modeling of the parallel mechanism is established, as shown in Figure 2.

The static coordinate system $o-xyz$ is established on the static platform ①. The coordinate origin o is the center of gravity of the static platform, and the x-axis coincides with the P_{11} axis. The x-axis rotates 90° anticlockwise around the origin o to be the y-axis, which has an angle of 30° with the axis of P_{21} . The z-axis is determined by the Cartesian coordinate system of the right hand. The coordinate system $o'-xyz$ is set on the top of the moving platform ②, and the coordinate origin o' is located on the top of the center of gravity D point of the moving platform ②, $o'D = l_4$. The u-axis coincides with P_{11} axis and points to C_1 . The u-axis rotates 90° anticlockwise around the origin o' to form the v-axis. The determination method of w-axis is the same as that of z-axis.

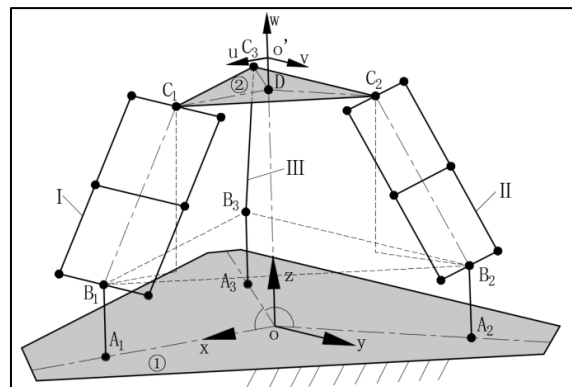


Figure 2. Kinematic Model of Parallel Mechanism

Set the scale parameters of the parallel mechanism: the distance between the initial position of the driving pair

P_{11}, P_{21} and P_{31} and the origin o are d_1, d_2 and d_3 respectively, that is, $oA_i = d_i$ ($i=1, 2, 3$, same below). The moving range of the driving pair is $[0, s_i]$. The length of each rod are $A_iB_i = l_1$, $B_iC_i = l_2$ and $C_iD = l_3$. The shape of moving platform is equilateral triangle, whose side length is $\sqrt{3}l_3$, and the size of each angle is $\angle A_i o A_j = \angle C_i D C_j = 120^\circ$. On account of $A_iB_i = l_1$, B_1, B_2 and B_3 are in the same plane and parallel to the xoy plane. Set the intermediate variable angle between B_iC_i and plane $B_1B_2B_3$ is α^* . The projection of B_iC_i on $B_1B_2B_3$ is $B_iC'_i$. The intermediate variable angle between $B_iC'_i$ and oA_i is β^* , where $i=1, 2, 3, j=1, 2, 3, i \neq j$, the schematic diagram of the angle position of the intermediate variable is shown in Figure 3.

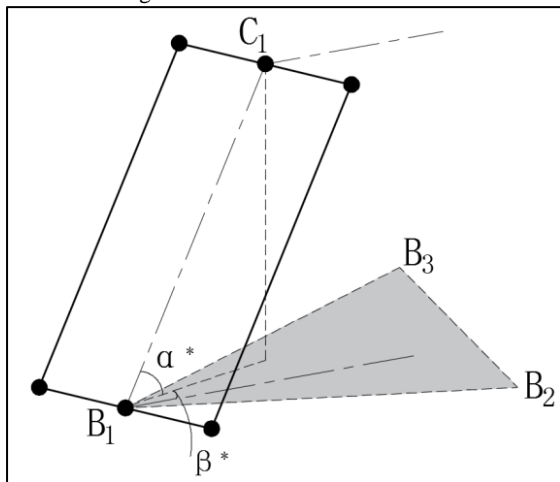


Figure 3. Schematic diagram of intermediate variable angle

4.2. Analysis of positive position solution of parallel mechanism

It is known that the motion range of the driving pair P_{11}, P_{21} and P_{31} are $[0, s_i]$ and the initial positions of them are d_1, d_2 and d_3 respectively. Next, we can use the condition to solve the coordinates (x, y, z) of o' on the moving platform ②.

According to the static coordinate system established by the kinematic model of the mechanism, the coordinates of each point can be obtained as follows:

$$\begin{aligned} &A_1(d_1 + s_1, 0, 0), B_1(d_1 + s_1, 0, l_1) \\ &A_2(-(d_2 + s_2)/2, \sqrt{3}(d_2 + s_2)/2, 0) \\ &B_2(-(d_2 + s_2)/2, \sqrt{3}(d_2 + s_2)/2, l_1) \\ &A_3(-(d_3 + s_3)/2, -\sqrt{3}(d_3 + s_3)/2, 0) \\ &B_3(-(d_3 + s_3)/2, -\sqrt{3}(d_3 + s_3)/2, l_1) \end{aligned}$$

(1) On the SOC of $\Delta_1=1$, using the intermediate variables angle α^* and angle β^* , the coordinate of C_1 and C_2 relative to the static coordinate system $o-xyz$ can be obtained by geometric method, that is

$$\begin{aligned} C_1^* &= \begin{bmatrix} d_1 + s_1 - l_2 \cos \alpha^* \cos \beta^* \\ l_2 \cos \alpha^* \sin \beta^* \\ l_1 + l_2 \sin \alpha^* \end{bmatrix} \\ C_2^* &= \begin{bmatrix} d_1 + s_1 - l_2 \cos \alpha^* \cos \beta^* - 3l_3/2 \\ l_2 \cos \alpha^* \sin \beta^* + \sqrt{3}l_3/2 \\ l_1 + l_2 \sin \alpha^* \end{bmatrix} \end{aligned}$$

(2) According to the position matrix of the moving coordinate system $o-uvw$ relative to the static coordinate system $o-xyz$, the position matrix of the moving coordinate system is

$${}^o p_{o'} = [x \quad y \quad z]^T \tag{6}$$

According to formula(6), combining the coordinates of C_1 and C_2 , we can get

$$C_1^* = C_1 + {}^o p_{o'}$$

On the SOC with $\Delta_2=-1$, the coordinates of C_1, C_2 and C_3 in the moving coordinate system $o-uvw$ are

$${}^o C_1(l_3, 0, -l_4), {}^o C_2(-l_3/2, \sqrt{3}l_3/2, -l_4),$$

$${}^o C_3(-l_3/2, -\sqrt{3}l_3/2, -l_4)$$

Coordinate of intermediate variable of point C_3^* is

$$C_3^* = \left(-\frac{l_3}{2} + x, -\frac{\sqrt{3}l_3}{2} + y, -l_4 + z \right)$$

By $B_2C_2 = B_3C_3 = l_2$, the constraint equation of parallel mechanism can be established:

$$\begin{cases} (x_{C_2}^* - x_{B_2})^2 + (y_{C_2}^* - y_{B_2})^2 + (z_{C_2}^* - z_{B_2})^2 = l_2^2 \\ (x_{C_3}^* - x_{B_3})^2 + (y_{C_3}^* - y_{B_3})^2 + (z_{C_3}^* - z_{B_3})^2 = l_2^2 \end{cases} \tag{7}$$

In this paper, we cleverly designed the moving platform of the parallel mechanism as an equilateral triangle, that is,

$$C_1C_2 = \sqrt{3}C_1D = \sqrt{3}l_3 \tag{8}$$

Because the equivalent relationship of the side length of the moving platform is known, the intermediate variables angle α^* and β^* can be solved by combining the link length constraint equation (7) of branch chain II and branch chain III. This is the key to solving the analytic expression of the positive position solution.

The coordinates of B_2 and C_2 are substituted into equation(7), which is sorted out and simplified, we can get

$$\begin{cases} A \cos \alpha^* \sin \beta^* + B \cos \alpha^* \cos \beta^* + C = 0 \\ D \cos \alpha^* \sin \beta^* + E \cos \alpha^* \cos \beta^* + F = 0 \end{cases}$$

where

$$A = \sqrt{3}l_2(l_3 - d_2 - s_2)$$

$$B = -2l_2[d_1 + s_1 + (d_2 + s_2 - 3l_3)/2]$$

$$C = [d_1 + s_1 + (d_2 + s_2 - 3l_3)/2]^2 + 3(l_3 - d_2 - s_2)^2/4$$

$$D = \sqrt{3}l_2(d_3 + s_3 - l_3)$$

$$E = -2l_2(d_1 + s_1 + (d_3 + s_3 - 3l_3)/2)$$

$$F = [d_1 + s_1 + (d_3 + s_3 - 3l_3)/2]^2 + 3(d_2 + s_2 - l_3)^2/4$$

By solving equation (7), we can get

$$\begin{cases} \beta^* = \arctan \frac{-BF - CE}{AF + CD} \\ \alpha^* = \arccos \frac{-C}{A \sin \beta + B \cos \beta} \end{cases}$$

Due to $C_i D = l_3$, substituting angle α^* and angle β^* into the coordinates of C_2^* , we can get the analytical formula (9) of the positive position solution of the o' point on the moving platform

$$\begin{cases} x = d_1 + s_1 - l_2 \cos \alpha^* \cos \beta^* - l_3 \\ y = l_2 \cos \alpha^* \sin \beta^* \\ z = l_1 + l_2 \sin \alpha^* + l_4 \end{cases} \quad (9)$$

4.3. Analysis of inverse solution position of parallel mechanism

Given the coordinates (x, y, z) of o' point in the moving coordinate system of moving platform (2), the distance $s_i (i=1,2,3)$ required to move the driving pair is calculated.

First, the absolute coordinates of point C_1, C_2 and C_3 are obtained:

$$C_1(x+l_3, y, z-l_4) \quad C_2\left(x-\frac{l_3}{2}, y+\frac{\sqrt{3}l_3}{2}, z-l_4\right) \\ C_3\left(x-\frac{l_3}{2}, y-\frac{\sqrt{3}l_3}{2}, z-l_4\right)$$

Owing to $B_i C_i = l_2 (i=1,2,3)$, we can establish constraint equation as follows:

$$\begin{cases} (x_{C_1} - x_{B_1})^2 + (y_{C_1} - y_{B_1})^2 + (z_{C_1} - z_{B_1})^2 = l_2^2 \\ (x_{C_2} - x_{B_2})^2 + (y_{C_2} - y_{B_2})^2 + (z_{C_2} - z_{B_2})^2 = l_2^2 \\ (x_{C_3} - x_{B_3})^2 + (y_{C_3} - y_{B_3})^2 + (z_{C_3} - z_{B_3})^2 = l_2^2 \end{cases} \quad (10)$$

Substituting the coordinates of point B_i and C_i into equation (10)

$$\begin{cases} s_1 = x + l_3 - d_1 \mp \sqrt{l_2^2 - y^2 - (z - l_4 - l_1)^2} \\ s_2 = \frac{-E_1 \pm \sqrt{E_1^2 - 4F_1}}{2} - d_2 \\ s_3 = \frac{-E_2 \pm \sqrt{E_2^2 - 4F_2}}{2} - d_3 \end{cases}$$

where

$$E_1 = x - \sqrt{3}y - 2l_3$$

$$E_2 = x - \sqrt{3}y + l_3$$

$$F_1 = (x - l_3/2)^2 + (y + \sqrt{3}l_3/2)^2 + (z - l_4 - l_1)^2 - l_2^2$$

$$F_2 = (x - l_3/2)^2 + (y - \sqrt{3}l_3/2)^2 + (z - l_4 - l_1)^2 - l_2^2$$

The results show that there are 8 groups of inverse solutions and 8 configurations of the mechanism.

4.4. Verification of positive and inverse analytical expressions of position for mechanism.

Set the scale parameters of the parallel mechanism as follows $l_1 = 50\text{mm}$, $l_2 = 400\text{mm}$, $l_3 = 60\text{mm}$, $l_4 = 60\text{mm}$, $d_1 = d_2 = d_3 = 60\text{mm}$.

Table 1. Positive solution value of mechanism position I

Coordinate	x/mm	y/mm	z/mm
Value	71.6565	17.3731	448.2069

Table 2. Inverse solution of mechanism position I

Serial number	s_1/mm	s_2/mm	s_3/mm
1	274.5280	170.7403	145.9299
2	274.5280	170.7403	-267.6775
3	274.5280	-232.3057	145.9299
4	274.5280	-232.3057	-267.6775
5	-151.2150	170.7403	145.9299
6	-151.2150	170.7403	-267.6775
7	-151.2150	-232.3057	145.9299
8	-151.2150	-232.3057	-267.6775

Set the moving range of the three driving pairs to be the same, all of which are $s_i \in [0, 350] (i=1,2,3)$. The scale parameters of the mechanism are substituted into the positive position solution(9). Take two sets of data respectively. Setting the first group data of driving pair are $s_1 = 274.2579\text{mm}$, $s_2 = 170.7403\text{mm}$, $s_3 = 145.9299\text{mm}$ respectively. Setting the second group data of coordinates of the moving platform is (71.6565, 17.3731, 448.2069). Take two groups of data respectively and use Matlab programming to calculate the positive solution of mechanism position, as shown in Table 1 and Table 2.

Take the data in Table 1 and substitute it into equation (10) to calculate the inverse position solution data of the mechanism, as shown in Table 2.

The results show that the positive and inverse solutions obtained by Matlab software are completely matched, which shows that the analytical formula of the positive and inverse position solutions of the parallel mechanism is correct.

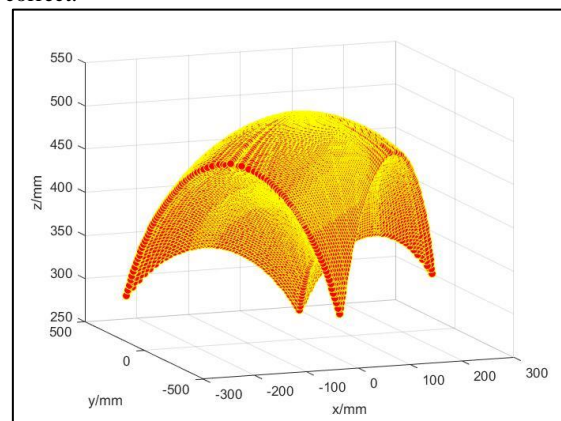


Figure 4. 3D figure of workplace for the mechanism

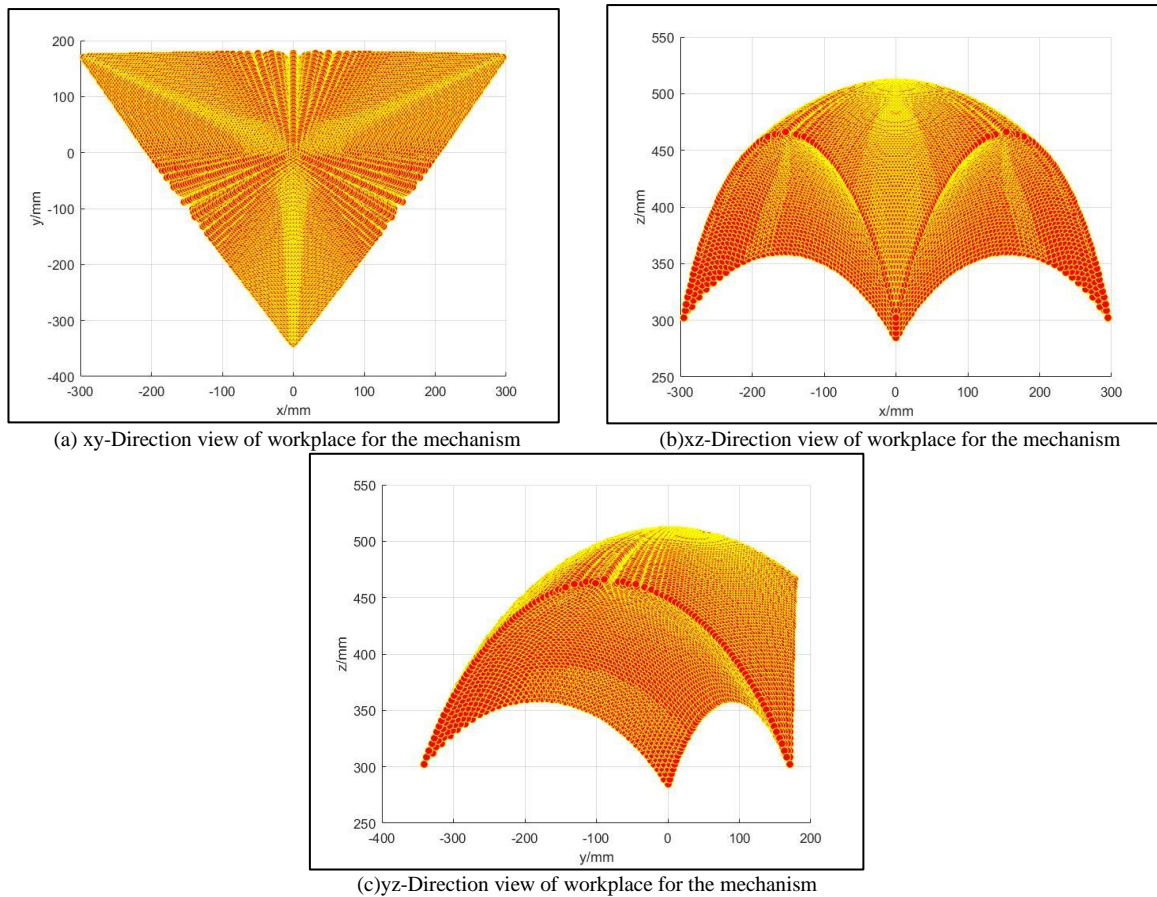


Figure 5. Three views of mechanism motion space

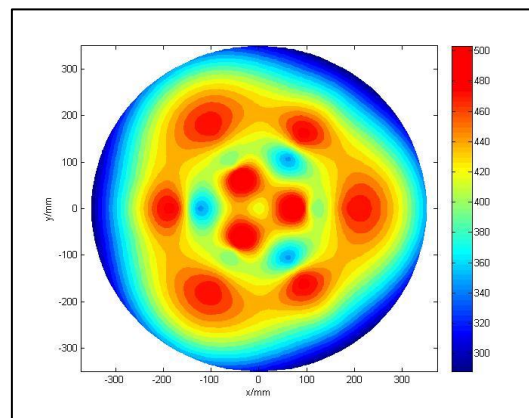


Figure 6. Cloud figure of workplace for the mechanism

5. Analysis of parallel mechanism motion performance

5.1. Workspace analysis

The motion range of driving pair P_{11} , P_{12} and P_{13} is set as $[0, 350\text{mm}]$, their initial position are $d_1=d_2=d_3=60\text{mm}$, and their step length are all 7mm . According to the positive analytical formula of mechanism (9), the stereogram and cloud diagram of working space of mechanism are obtained by Matlab software programming, as shown in Fig. 4, Fig. 5 and Fig. 6.

Analysis of Fig. 4, Fig. 5 and Fig.6 shows that:

1) The workspace of the parallel mechanism is symmetrically distributed, continuous and free of cavities, with good performance. When all three driving pairs are at

the starting point, the mechanism reaches the workspace boundary.

2) Within the set range of the working stroke of the mechanism driving pair, the working space does not contain singular points, the effective working space is large and the range is centralized, which has a good use value.

5.2. Singularity analysis of parallel mechanism

5.2.1. Singularity principle of parallel mechanism

By analyzing whether the determinant of Jacobian matrix is zero, we can judge whether the mechanism is singular. The singular configuration of parallel mechanism can be divided into three categories: (1) the input

singularity will occur when the $|J_q|=0$ and $|J_p| \neq 0$; (2) the output singularity will occur when the $|J_p|=0$ and $|J_q| \neq 0$; (3) the comprehensive singularity will occur when the $|J_q|=0$ and $|J_p|=0$. The drive range of the parallel mechanism should be avoided near the singular location.

Both sides of the constraint equation (10) of the link length of the mechanism derive the time at the same time, and the relationship between the output speed $v = [\dot{x} \ \dot{y} \ \dot{z}]^T$ of the end platform of the mechanism and the input speed $\dot{x} = [\dot{s}_1 \ \dot{s}_2 \ \dot{s}_3]^T$ of the driving pair is obtained as follows

$$J_p v = J_q \dot{x} \tag{11}$$

where

$$J_p = \begin{bmatrix} v_{11} & v_{12} & v_{13} \\ v_{21} & v_{22} & v_{23} \\ v_{31} & v_{32} & v_{33} \end{bmatrix} \tag{12}$$

$$J_q = \text{diag}(u_{11}, u_{22}, u_{33}) \tag{13}$$

$$\begin{aligned} v_{11} &= x_{B_1} - x_{C_1}, & v_{12} &= y_{B_1} - y_{C_1}, & v_{13} &= z_{B_1} - z_{C_1}, \\ v_{21} &= x_{B_2} - x_{C_2}, & v_{22} &= y_{B_2} - y_{C_2}, & v_{23} &= z_{B_2} - z_{C_2}, \\ v_{31} &= x_{B_3} - x_{C_3}, & v_{32} &= y_{B_3} - y_{C_3}, & v_{33} &= z_{B_3} - z_{C_3}, \\ u_{11} &= (x_{B_1} - x_{C_1})s_1, \\ u_{22} &= s_2(x_{C_2} - x_{B_2})/2 + \sqrt{3}s_2(y_{C_2} - y_{B_2})/2 \\ u_{33} &= s_3(x_{C_3} - x_{B_3})/2 - \sqrt{3}s_3(y_{C_3} - y_{B_3})/2 \end{aligned}$$

5.2.2. Input singularity

If any element of the diagonal of equation (12) is zero, the input singularity of the mechanism will occur when $|J_q|=0$ and $|J_p| \neq 0$.

Owing to $u_1=0, u_2=0, u_3=0$, we can obtain

$$\left. \begin{aligned} x_{B_1} &= x_{C_1} \\ x_{C_2} &= x_{B_2}, y_{C_2} = y_{B_2} \\ x_{C_3} &= x_{B_3}, y_{C_3} = y_{B_3} \end{aligned} \right\} \tag{14}$$

When the coordinate of the $B_i (i=1,2,3)$ and $C_i (i=1,2,3)$ satisfies any equation in the formula (14), then $|J_q|=0$. In other words, A_i, B_i and $C_i (i=1,2,3)$ are collinear, the input singularity occurs. It indicates that the moving platform of the parallel mechanism reaches the boundary of the workspace.

5.2.3. Output singularity

The output singularity of the parallel mechanism will occur when $|J_p|=0$ and $|J_q| \neq 0$. In other words, the driving pair can't drive the moving platform even if the force on the moving platform is very small. If we regard the corresponding row of formula (12) as a vector, we can get

$$J_p = [V_1 \ V_2 \ V_3]^T$$

1. When any two vectors are linearly related, $|J_p|$ equals zero.

Setting $V_1 = \eta V_2$ (where η is a coefficient), B_1C_1 and B_2C_2 are parallel in space, that is $[v_{11} \ v_{12} \ v_{13}] = \eta [v_{21} \ v_{22} \ v_{23}]$

2. When the three vectors are linearly correlated, $|J_p|$ equals zero.

Setting $V_1 = \eta_1 V_2 + \eta_2 V_3$ (where η_1 and η_2 are coefficient), B_1C_1, B_2C_2 and B_3C_3 are parallel in space, that is $[v_{11} \ v_{12} \ v_{13}] = \eta_1 [v_{21} \ v_{22} \ v_{23}] = \eta_2 [v_{31} \ v_{32} \ v_{33}]$.

5.3. Comprehensive singularity

The mechanism will have synthetic singularity when $|J_q|=0$ and $|J_p|=0$, that is, input singularity and output singularity occur at the same time, and the mechanism satisfies A_i, B_i and C_i three-point collinear and $B_iC_i // B_jC_j (i=1, 2, 3, j=1, 2, 3 \text{ and } i \neq j)$.

6. Driving significance analysis

6.1. Orthogonal test scheme design and range analysis

It can be seen from equation (9) that the drive of the mechanism leads to the nonlinear change of the coordinates of the moving platform. Therefore, in the whole driving range, the driving change has little influence on the coordinate increment of the moving platform. In other words, we look for the driving range with the largest reduction of displacement, which is convenient for the real-time control of the parallel mechanism. Therefore, the optimal driving range of the parallel mechanism is solved by designing the orthogonal experiment. Taking the coordinate difference of the moving platform of the parallel mechanism as the research object, the significant influence of the driving pair on the coordinate change of the moving platform is explored. The target parameters of the test object are the changes of the coordinates of the moving platform $\Delta x, \Delta y$ and Δz . The structural parameters expressing the coordinate change of the moving platform are the increments of s_1, s_2 and s_3 , the increment equal $s = 70\text{mm}$.

The starting points of the five increments of the three drivers are 0, 70mm, 140mm, 210mm, 280mm, respectively. It is assumed that there is no interaction between the three driving displacements in the control process [28].

The orthogonal Table $L_p(t^q)$ is used to arrange the experiment, where L is the code of the orthogonal table, p is the number of experiments, t is the horizontal number, and q is the number of influencing factors. In this paper, the orthogonal table $q=3$, is selected as shown in Table 3.

Table 3. Values of s_1, s_2 and s_3 at different levels in orthogonal tests

Level	s_1/mm	s_2/mm	s_3/mm
1	0	0	0
2	70	70	70
3	140	140	140
4	210	210	210
5	280	280	280

The results of orthogonal test were analyzed, as shown in Table 4. Calculate the numerical value and range of the three factors under the five levels, and test whether the j^{th} column factor has significant influence on the test result statistic F_j . Under the given significance level α , if

$F_j \geq F_{1-\alpha}(f_j, f_e)$ is satisfied, it can be considered that the factors arranged in this column have a significant influence on the coordinate change of the moving platform of the mechanism, otherwise, the influence is not significant.

Table 4. Range analysis

Test	The influence of driving on x				The influence of driving on y				The influence of driving on z			
	s_1	s_2	s_3	Error term	s_1	s_2	s_3	Error term	s_1	s_2	s_3	Error term
K_{1j}	94.93	-47.47	-56.74	4.27	0.00	82.21	-98.28	-8.52	-116.18	-116.18	-112.66	-199.34
K_{2j}	-28.79	-43.61	-2.30	-37.92	-13.16	-20.43	-3.99	5.15	-156.12	-132.29	-162.51	-182.71
K_{3j}	-41.66	19.09	8.36	-56.75	-2.02	-37.09	14.47	6.87	-180.44	-180.44	-189.85	-173.60
K_{4j}	-79.32	15.02	13.53	-3.02	9.54	-29.10	23.43	0.70	-184.91	-208.73	-215.91	-166.16
K_{5j}	-11.35	-9.23	-29.24	27.22	-17.21	-18.44	41.51	-27.02	-253.73	-253.73	-210.43	-169.57
R_j	174.26	66.55	70.27	83.97	26.75	119.30	139.78	33.92	137.55	137.55	103.24	33.18

6.2. Significance analysis

According to the orthogonal test scheme and range analysis method, the orthogonal influence factors are used for numerical calculation to obtain 25 sets of orthogonal combination values as shown in Table 5.

Table 5. Numerical results of orthogonal test combination

Level	1	2	3	$\Delta x/mm$	$\Delta y/mm$	$\Delta z/mm$
1	1	1	1	0.00	0.00	-7.96
2	1	2	1	11.06	0.00	-15.67
3	1	3	3	21.24	0.00	-22.33
4	1	4	4	28.58	0.00	-29.57
5	1	5	5	34.04	0.00	-40.66
6	2	1	2	-5.53	9.58	-15.67
7	2	2	3	-0.76	-1.32	-26.10
8	2	3	4	3.55	-2.64	-36.95
9	2	4	5	8.10	-2.89	-50.81
10	2	5	1	-34.14	-15.89	-26.59
11	3	1	3	-10.62	18.39	-22.33
12	3	2	4	-4.06	1.75	-36.95
13	3	3	5	-1.00	-1.73	-51.33
14	3	4	1	-19.04	-18.93	-25.76
15	3	5	2	-6.95	-1.50	-44.07
16	4	1	4	-14.29	24.75	-29.57
17	4	2	5	-53.16	16.65	-26.98
18	4	3	1	-6.87	-25.95	-25.76
19	4	4	2	-3.06	-5.30	-43.04
20	4	5	3	-1.94	-0.61	-59.55
21	5	1	5	-17.02	29.48	-40.66
22	5	2	1	3.31	-37.51	-26.59
23	5	3	2	2.17	-6.77	-44.07
24	5	4	3	0.44	-1.99	-59.55
25	5	5	4	-0.25	-0.43	-82.86

The data were processed according to the method of variance analysis. The statistic used to test whether the driving increment of the j -th column has a significant effect on the dynamic platform increment is F_j . According to the F distribution Table, we can get $F_{0.90}(4,8) = 2.81$, $F_{0.95}(4,8) = 3.84$ and $F_{0.99}(4,8) = 7.01$. The statistics of the increment Δx of the x-coordinate of the moving platform corresponding to the three driving

increments are, $F_{\Delta x \Delta s_1} = 6.58$, $F_{\Delta x \Delta s_2} = 1.52$ and $F_{\Delta x \Delta s_3} = 1.32$ respectively. Under the significance level of $\alpha = 0.05$, the increase of s_1 has a significant effect on the change of moving platform coordinate Δx , while s_2 and s_3 have no significant effect on the change of moving platform coordinate Δx .

The statistics of the increment Δy of the y-coordinate of the moving platform corresponding to the three driving increments are $F_{\Delta y \Delta s_1} = 1.04$, $F_{\Delta y \Delta s_2} = 21.78$, $F_{\Delta y \Delta s_3} = 27.24$ respectively. Under the significance level of $\alpha = 0.01$, the increase of s_1 has no significant effect on the change of moving platform coordinate Δy , while s_2 and s_3 have significant influence on the change of moving platform y-coordinate, and the order of significant influence is as follows s_3, s_2 .

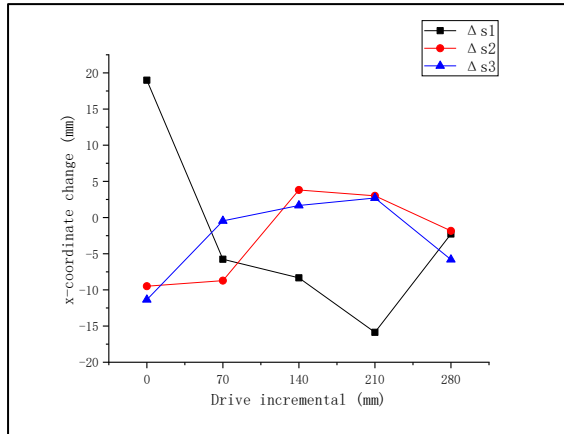
The statistics of the increment Δz of the z-coordinate of the moving platform corresponding to the three driving increments are, $F_{\Delta z \Delta s_1} = 1.04$, $F_{\Delta z \Delta s_2} = 21.78$, $F_{\Delta z \Delta s_3} = 27.24$, respectively. Under the significance level of $\alpha = 0.01$, the three drives have significant effects on the changes of the moving platform, and the order of significant influence are s_2, s_1 , and s_3 .

6.3. Analysis of the change characteristics of target parameters

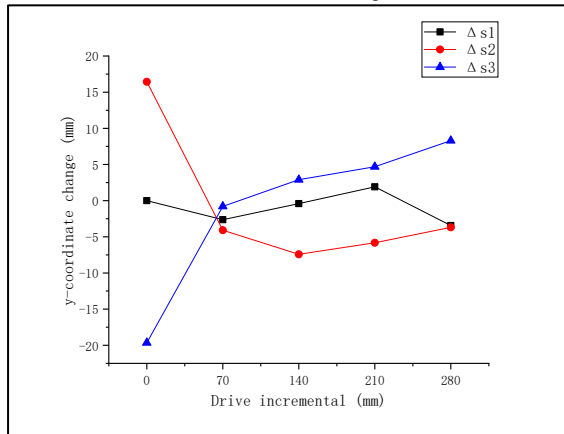
In order to more intuitively analyze the influence of each factor level on the coordinate increment of the moving platform, we can comprehensively analyze the results according to the orthogonal test theory¹⁹. Sum the results of calculation at the level of each driving increment, and then calculate the average value. We can draw a graph of the influence of the driving on the coordinates of the moving platform, as shown in Figure 7.

As can be seen from fig. 7 (a), with the increase of s_1 , the influence on the x-coordinate Δx of the moving platform decreases at first and then increases, and its variation range is (-15.9mm,19.0mm).. With the increase of s_2 and s_3 , their influences on the x-coordinate Δx of the moving platform increase at first and then decrease, and their variation ranges are smaller, which are (-

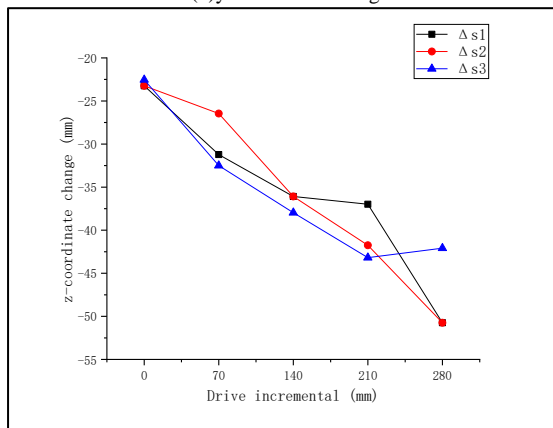
9.5mm,3.8mm) and (-11.3mm,2.7mm) respectively. Therefore, it is easier to control the change of the x-coordinate of the moving platform by selecting the drive s_1 .



(a) x-coordinate change



(b) y-coordinate change



(c) z-coordinate change

Figure 7. Coordinate increment of moving platform changes with driving increment.

As can be seen from fig. 7 (b), with the increase of s_1 , the influence on the y-coordinate Δy of the moving platform fluctuates in a very small range, and its variation range is (-3.4mm, 1.9mm). With the increase of s_2 , the influence on the y-coordinate Δy of the moving platform decreases at first, and then tends to smooth, and its variation range is (-3.7mm, 1.9mm). With the increase of

s_3 , the influence on the y-coordinate Δy of the moving platform increases at first and then tends to smooth, and its variation range is (-7.42mm, 16.44mm). Therefore, driving s_2 and s_3 can control the y-coordinate of the moving platform more easily.

As can be seen from fig. 7(c), with the increase of s_1 , s_2 and s_3 , the z-coordinate Δz of the moving platform all show a downward trend, and their changing ranges are (-50.75mm, -23.24mm), (-50.75mm, -23.24mm) and (-43.18mm, -22.53mm), respectively. Therefore, driving s_1 , s_2 and s_3 can effectively control the z-coordinates of the moving platform.

According to the comprehensive balance principle, the optimal driving range of the parallel mechanism is (70mm, 350mm). The influence of the driving increment on the coordinate increment of the moving platform can provide a reference basis for the real-time control and further optimization analysis of the parallel mechanism.

7. Experimental results and analysis

The physical prototype model is made according to the mechanism parameters of simulation analysis, as shown in Figure 8. The theoretical basis of significance analysis is the analytical formula of forward kinematics solution. Therefore, it is necessary to verify the correctness of equation (9) through experiments. It can be seen from Figure 7 that the driving increment has the greatest impact on the displacement of z-axis of the moving platform. Therefore, the z-axis displacement of the moving platform is selected for experimental verification.



Figure 8. Physical prototype model of 2PPa-PSS PM

Firstly, the moving pairs P_1 , P_2 and P_3 are set at the initial position, and then the displacement in the Z direction of the end platform is measured by the laser rangefinder, to verify the correctness of the analytical formula of the forward kinematics solution. In addition, the accuracy of the laser rangefinder is 1mm. The experimental results are compared with the theoretical analysis, as shown in Figure 9.

According to Fig. 7(c), the three moving pairs have the same influence on the displacement of the moving platform in the Z direction, which is also proved by the experimental test results. According to figure 9, within the

driving range of [0, 150mm], the coordinate changes in the Z direction of the moving platform are basically the same. The correctness of equation (9) is verified.

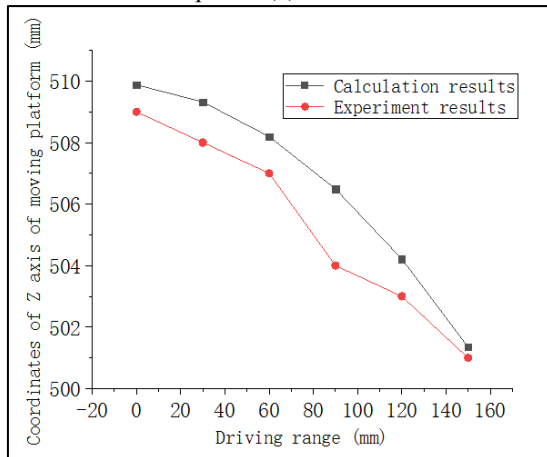


Figure 9. Z-axis displacement of 2PPa-PSS PM moving platform

8. Conclusions

The main conclusions are as follows:

1. The topological structure characteristics of a low coupling degree 3T PM are analyzed, and it is concluded that the degree of freedom is 3 and the coupling degree is 1. The kinematics model is established, and the analytical formula of positive and inverse position solution of the PM is solved based on the sequential single open chain method. The correctness of the analytical formula is verified by numerical calculation.

2. Based on the analytical formula of positive position solution, the complete discrete point workspace of the PM is obtained. The workspace of the PM is large and there is no cavity in the interior. Then, the singular configuration of the mechanism is analyzed based on the analytic expression of the inverse position solution.

3. The orthogonal test scheme is designed, and the coordinate change of the moving platform is numerically simulated. At different levels of the orthogonal experimental design, the three driving increments have significant effects on the coordinate changes of the moving platform. Finally, it is concluded that the optimal driving range of the parallel mechanism is 70mm - 350mm.

Declaration of conflicting interests

The author(s) declared no potential conflicts of interest with respect to the research, authorship, and /or publication of this article.

Funding

The author(s) disclosed receipt of the following financial support for the research, authorship, and/or publication of this article: The work was supported by the Guangxi Natural Science Foundation of China [2018GXNSFBA281080].

Reference

[1] Ranjan, J.; Damien, C.; Luc, B.; Fabrice, R.; Guillaume M.;

- "Workspace, joint space and singularities of a family of delta-like robot", *Mechanism and Machine Theory*, 127, pp. 73-95, 2018.
<https://doi.org/10.1016/j.mechmachtheory.2018.05.004>
- [2] Zhao J.; Wu C, C.; Yang, G, L.; Chen C, Y.; Chen S, L.; Xiong C, Y.; Zhang C.; "Kinematics analysis and workspace optimization for a 4-DOF 3T1R parallel manipulator". *Mechanism and Machine Theory*, 167, 2022, 104484.
<https://doi.org/10.1016/j.mechmachtheory.2021.104484>
- [3] Xu LM.; Chen QH.; He LY.; Li QC.; "Kinematic analysis and design of a novel 3T1R 2-(PRR)2RH hybrid manipulator". *Mechanism and Machine Theory*, 112, pp. 105-122, 2017.
<https://doi.org/10.1016/j.mechmachtheory.2017.01.009>
- [4] Masoud, Z.; Nazzal, M.; Alhazza, K.; "Multimode input shaping control of flexible robotic manipulators using frequency-modulation". *Jordan Journal of Mechanical and Industrial Engineering*, 10(3), pp. 179-188, 2016.
<http://jjmie.hu.edu.jo/vol%2010-3/JJMIE-137-15-F-1.pdf>
- [5] Gong J, J.; Wei, W.; Cai G, W.; Liu Y, X.; Peng S, X.; "Kinematic Performance Analysis of a Controllable Mechanism Welding Robot with Joint Clearance". 2020 4th International Conference on Measurement Instrumentation and Electronics, Chengdu, People's Republic of China, 2020.
<https://doi.org/10.1051/mateconf/202032703006>
- [6] Mohammad, Al-K.; Omar, B.; Ibrahim Al-A.; "Exploration algorithm technique for multi-robot collaboration". *Jordan Journal of Mechanical and Industrial Engineering*, 5(2), pp. 177-184, 2011.
[http://jjmie.hu.edu.jo/files/v5n2/JJMIE-47-11%20Revised%20Adawan\(10\).pdf](http://jjmie.hu.edu.jo/files/v5n2/JJMIE-47-11%20Revised%20Adawan(10).pdf)
- [7] Gregorio, R. D.; "Kinematics of a new spherical manipulator with three equal legs: The 3-URC wrist". *Robotic System*, 18(5), pp.213-219, 2001.
<https://doi.org/10.1002/rob.1017>
- [8] Stock, M., Miller, K.; "Optimal Kinematic Design of Spatial Parallel Manipulators: Application to Linear Delta Robot". *Journal of Mechanical Design*, 125(2), pp. 292-301, 2003.
<https://doi.org/10.1115/1.1563632>
- [9] Luo, X.; Xie, F. G.; Liu, X. J.; "Kinematic calibration of the 3-degree-of-freedom redundantly actuated spatial parallel module of a five-axis hybrid machine". *Proceedings of the Institution of Mechanical Engineers, Part B: Journal of Engineering Manufacture*, 234(9), pp. 1185-1197, 2020.
<https://doi.org/10.1177/0954405420911299>
- [10] Zhang, F.X.; Chen, S. L.; He, Y. Y.; Ye, G. Y.; Zhang, C.; Yang, G, L.; "A Kinematic Calibration Method of a 3T1R 4-Degree-of-Freedom Symmetrical Parallel Manipulator". *Symmetry*, 12(3), pp. 1-16, 2020.
<https://doi.org/10.3390/sym12030357>
- [11] Deng, J. M.; Wang, W.; Shen, H. P.; Ma Z. H.; Li, Y. F.; Duan, S. L.; "Research on a Novel 3-DOF Planar Parallel Manipulator Driven by Three-Slider and its Larger Workspace Analysis". *Applied Mechanics and Materials*, 1503, pp. 590-593, 2012.
<https://doi.org/10.4028/www.scientific.net/AMM.130-134.590>
- [12] Li, Y. W.; Wang, J. S.; Liu, X. J.; Wang, L. P.; "Dynamic performance comparison and counterweight optimization of two 3-DOF parallel manipulators for a new hybrid machine tool". *Mechanism and Machine Theory*, 45(11), pp. 1668-1680, 2010.
<https://doi.org/10.1016/j.mechmachtheory.2010.06.009>
- [13] Latifah, N.; Stéphane C.; Philippe, Wenger.; Josef, S.; Manfred, H.; "Reconfiguration analysis of a 4-RUU parallel manipulator". *Mechanism and Machine Theory*, 96(2), pp. 269-289, 2016.
<https://doi.org/10.1016/j.mechmachtheory.2015.09.004>
- [14] Kelaiaia, R.; Company, O.; Zaatri, A.; "Multiobjective Optimazation of a Linear Delta Parallel Robot". *Mechanism and Machine Theory*, 50(2), pp. 159-178, 2012.
<https://doi.org/10.1016/j.mechmachtheory.2011.11.004>
- [15] Ma, K.; Ma, H.; Tian, H.; "Kinematic analysis of a novel 2-PrRS-PR(P)S metamorphic parallel mechanism". *Advances in Mechanical Engineering*, 11(11), pp. 1-15, 2019.
<https://doi.org/10.1177/1687814019889776>

- [16] Arian, A.; Danaei, B.; Abdi, H.; Nahavandi, S.; "Kinematic and dynamic analysis of the Gantry-Tau, a 3-DOF translational parallel manipulator". *Applied Mathematical Modelling*, 51, pp. 217-231, 2017. <https://doi.org/10.1016/j.apm.2017.06.012>
- [17] Cuan-Urquiza, E.; Rodriguez-Leal, E.; "Kinematic analysis of the 3-CUP parallel mechanism". *Robotics and Computer-Integrated Manufacturing*, 29(5), pp. 382-395, 2013. <https://doi.org/10.1016/j.rcim.2013.03.002>
- [18] Zeng, Q.; Ehmman, K. F.; Cao, J.; "Tri-pyramid Robot: Design and kinematic analysis of a 3-DOF translational parallel manipulator", *Robotics and Computer-Integrated Manufacturing*, 30(6), pp. 648-657, 2014. <https://doi.org/10.1016/j.rcim.2014.06.002>
- [19] Zeng, Q.; Ehmman, K. F.; Cao, J.; "Tri-pyramid Robot: stiffness modeling of a 3-DOF translational parallel manipulator". *Robotica*, 34(2), pp. 383-402, 2016. <https://doi.org/10.1017/S0263574714001520>
- [20] Liu, X, L.; Wang, Q, Q.; Malikov, A.; Wang, H, R.; "The design and dynamic analysis of a novel 6-DOF parallel mechanism". *International Journal of Machine Learning and Cybernetics*, 3(1), pp. 27-37, 2012. <https://doi.org/10.1007/s13042-011-0040-1>
- [21] Yan, Y.; Luo, YF.; Shi, ZX.; Yao, WK.; Yang, TL.; "Structure synthesis of two-translation and two-rotation parallel mechanisms based on the POC-based approach". 1st International Conference on Mechanical Engineering, Phuket, Thailand, 2011. <https://doi.org/10.4028/www.scientific.net/AMM.52-54.759>
- [22] Zeng, D, X.; Huang, Z.; "Type synthesis of the rotational decoupled parallel mechanism based on screw theory". *Science China-Technological Sciences*, 54(4), pp. 998-1004, 2011. <https://doi.org/10.1007/s11431-010-4239-2>
- [23] Zeng, D, X.; Jing, G, N. ; Su, Y, L.; Wang, Y.; Hou, Y, L.; "A novel decoupled parallel mechanism with two translational and one rotational degree of freedom and its performance indices analysis". *Advances in Mechanical Engineering*, 8(5), pp. 1-10, 2016. <http://doi.org/10.1177/1687814016646936>
- [24] Zeng, D, X.; Hou, Y, L.; Lu, W, J.; Huang, Z.; "Comparative Analysis of Characteristics of the Coupled and Decoupled Parallel Mechanisms". *Chinese Journal of Mechanical Engineering*, 23(4), pp. 468-476, 2010. <http://doi.org/10.3901/CJME.2010.04.468>
- [25] Yang T, L.;Liu, X, A.; Shen, H, P., HangL, B.; Luo Y, F.; Jin Q.; "Topology Design of Robot Mechanisms".Springer, Singapore, 2018. <http://doi.org/10.1007/978-981-10-5532-4>
- [26] Hou, Y, L.; Zeng, D, X.; Zhang, Z, Y.; Wang, C, M.; Hu, X, Z.; "A Novel Two Degrees of Freedom Rotational Decoupled Parallel Mechanism". 2nd International Conference on Advanced Design and Manufacturing Engineering, Taiyuan, People's Republic of China, 2012. <http://doi.org/10.4028/www.scientific.net/AMM.215-216.293>
- [27] Yu, S, S.; Zhang, J, J.; Li, W, M.; Yang, X, H.; "New Decoupled 2-Dof Parallel Mechanism with Fully Spherical Workspace".5th Annual International Conference on Information System and Artificial Intelligence, Zhejiang, People's Republic of China, 2020. <http://doi.org/10.1088/1742-6596/1575/1/012104>
- [28] Shu, L. S., Wang, B., He, Y. Y., "Optimization of Process Parameters of Laser Cladding 304L Alloy Powder Based on Orthogonal Experiment".*Mechanical Engineering Science*, 1(2), pp. 18-24, 2019. <https://doi.org/10.33142/me.v1i2.1656>